Optical probes of elementary excitations in quantum dots

Pawel Hawrylak
Institute for Microstructural Sciences
National Research Council of Canada
Ottawa, Canada K1A OR6.

Received February 2, 1997

The intraband and interband optical probes of elementary excitations in quantum dots containing electrons or excitons are discussed. The ground state properties and charge and spin excitations in self-assembled and deep etched dots are obtained through exact diagonalization techniques, Hartree-Fock, and Hartree calculations. The calculations of far infrared, interband, and inelastic light scattering spectroscopies are compared with experiments.
PACS numbers: 73.20Dx, 71.35;Ji, 78.20Ls, 78.66Fd

I. Introduction

The reduction in size of electronic and optoelectronic devices leads to Quantum Dot(QD) based single-electron transistors(QSET) [1] and single-exciton lasers(QDL) [2]. Because of reduced dimensionality the interaction among carriers in QD is of paramount importance. We use Hartree, Hartree-Fock, and exact diagonalization methods to study ground state properties and elementary excitation in quantum dots as a function of the number of carriers N. Varying N often leads to drastic changes in electronic properties of QSET and QDL. To understand these properties it is necessary to calculate the coupling of elementary excitations to external probes. In the intraband far infrared spectroscopy absorption of photons couples to the center of mass motion, and through boundaries or imperfections, to relative motion of electrons determined by electron-electron interactions. In interband spectroscopy excess electrons interact with an exciton. An electron component of an exciton can be viewed as a charge and spin excitation of the electron system. In a quantum dot laser adding/removing an exciton can be viewed as a one-particle probe of a many-exciton excitation spectrum. In inelastic light scattering one probes directly charge and spin density excitation spectrum.

We review here briefly our work on elementary excitation in quantum dots and their coupling to optical probes. The calculated response functions are compared with available far infrared, photoluminescence and electronic Raman experiments.

II. Self-assembled dots

Self-Assembled Dots (SAD) [3] are small quasi-two-dimensional semiconductor structures formed spontaneously during epitaxial growth of strained layers. Dots in the shape of pyramids [4,5], disks [6], and lenses [7-10] have been reported, although the actual determination of the shape is not definite. The SADs described here are the lens-shaped structures formed on a narrow InGaAs wetting layer (WL) and surrounded by the GaAs barriers [7-10]. The dependence of energy levels of SAD on side, depth of confining potential, and the magnetic field has been studied in Ref. [11]. The effects of electron-electron and electron-hole interactions on electronic and optical properties of SAD containing many electrons and/or excitons have been investigated theoretically [12,13] and experimentally [4,10,14,15]. The Single Electron Capacitance (SECS), far-infra-red (FIR), and photoluminescence/absorption spectra were calculated as a function of the number of particles, the size, and the magnetic field [12]. Results were compared with SECS and FIR experiments [7,8] and PL experiments by Raymond et al [10].

A. Single particle states

A schematic picture of a lens-shaped $In_{0.5}Ga_{0.5}As$ SAD is shown in Fig. 1. The dot forms on a wetting layer (WL) of thickness t_w, in the form of a part of a sphere with fixed height h and radius at the base s. The carriers, confined to a narrow WL quantum well are further localized in the area of the dot due to the effectively increased thickness of the layer. The effective 2D potential acting on carriers is shown in Fig. 1b. It's radial dependence can be very well approximated by a parabola, and electronic states can be approximated by Fock-Darwin states. This is shown in Fig. 1c where numerically calculated energy levels are shown as a function of angular momentum. The calculated levels tend to bunch into groups, forming well separated shells. The spacing of energy levels and the wavefunctions are very well fitted by Fock-Darwin energy levels, as discussed below. The FD states $|nm>= (a^\dagger)n(b^\dagger)^m|00> /\sqrt{n!m!}$ are those of a pair of harmonic oscillators with energies $\Omega_\pm = \frac{1}{2}(\Omega \pm \omega_c)$, where: $\Omega^2 = \omega_0^2 + 4\omega_c^2$, $\omega_c = eB/cm_e$ is the cyclotron energy, and ω_0 measures the effective confinement energy. Associating index n with frequency Ω_+ and index m with frequency Ω_-, the energy E^e_{nm} and orbital angular momentum R_{nm} of the state $|nm>$ are: $R_{nm} = m-n$ and $E^e_{nm} = \Omega_+(n+1/2)+\Omega_-(m+1/2)$ The Zeeman energy is very small and can be neglected. The eigenstates are doubly degenerate due to spin σ. The valence band holes are treated in the effective mass approximation as positively charged particles with angular momentum $R^h_{mn} = n - m$, opposite to the electron, and FD energies $E^h_{mn} = \Omega^h_+(n + 1/2) + \Omega^h_-(m + 1/2)$ (ignoring the semiconductor gap EG). The knowleadge of single particle states allows us to proceed to the calculation of many-body effects.

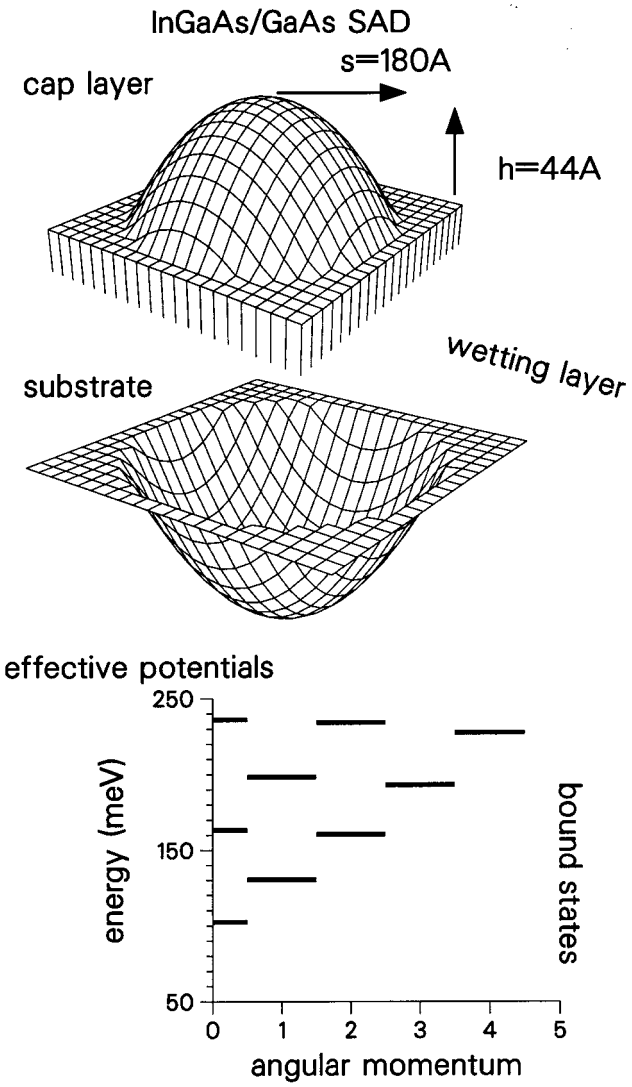

Figure 1. (a) schematic picture of the InGaAs/GaAs self assembled dot (b) effective lateral confining potential for electrons (c) calculated energy levels.

B. Many-particle states

With a composite index $j = [m, n, \sigma]$ describing the FD states the Hamiltonian of the interacting electron (electron-hole) system may be written in a compact form:

$$H = \sum_i E^e_i c^+_i c_i + \sum_i E^h_i h^+_i h_i - \sum_{ijkl} < ij|v_{eh}|kl > c^+_i h^+_j h_k c_l$$
$$+\frac{1}{2}\sum_{ijkl} < ij|v_{ee}|kl > c^+_i c^+_j c_k c_l + \frac{1}{2}\sum_{ijkl} < ij|v_{hh}kl > h^+_i h^+_j h_k h_l . \quad (1)$$

The operators $c_i^+(c_i)$, $h_i^+(h_i)$ create (annihilate) the electron or valence band hole in the state $|i>$ with the single-particle energy E_i. The two-body Coulomb matrix elements are $< ij|v|kl >$ for electron-electron (ee), hole-hole (hh) and electron-hole (eh) scattering, respectively [16,17].

The eigenstates $|\nu>$ of the electron(electron-hole) system with N electrons(excitons) are expanded in products of the electron and hole configurations $|\nu>= (\Pi_{j+1}^N c_j^+)(\Pi_{k=1}^N h_k^+)|v>$. Up to 30 single particle states per dot, including spin, were used in calculations. The electronic configurations were labeled by total angular momentum R_{tot} and z-th component of total spin S_z^{tot}. For electrons, numerical diagonalization of up to $N = 6$ electrons was carried out for Hilbert spaces with different total angular momentum. For excitons, we concentrated on the optically active subspace of $R_{tot} = 0$ and $S_z^{tot} = 0$. A combination of exact diagonalization techniques (for up to $N = 6$ excitons) in configuration space coupled with the Hartree-Fock approximation extended calculations up to $N = 20$ excitons.

C. Electronic shells

Due to the large quantization of kinetic energy the electronic shells correspond to the minimum kinetic energy configuration. In case of partially filled shells i.e. degenerate states the configurations with maximum total spin and maximum individual momentum form the ground state. The calculated evolution of the total angular momentum and spin of the ground state as a function of the number of electrons is shown in Fig. 2. For example, we fill up the d shell orbitals with spin down electrons as $|2,0>$, $|0,2>$, $|1,1>$ etc. This trend is in agreement with Hund's rules.

The role of degeneracies, spin, electron-electron interactions and the magnetic field can be illustrated for $N = 4$ electrons, i.e. two electrons in a partially filled p-shell. For low magnetic fields the two "core electrons" of the s-shell are frozen in a spin singlet state while the two electrons on the p-shell occupy degenerate FD orbitals $|01>$ and $|10>$. The ground state is a spin triplet, zero total angular momentum state $R = 0$,$S = 1$. The triplet state lowers it's energy by exchange-interaction term $< 01;10|V_{ee}|01;10 >$ while the spin singlet state $R = 0$, $S = 0$ increases it's energy by the same amount. With increasing magnetic field the triplet state $R = 0$, $S = 1$ begins to compete with a finite angular momentum spin singlet state $R = 2$, $S = 0$. In the $R = 2$ state both p electrons occupy the lower energy orbital $|10>$. At $B \approx 2.8$ Tesla the gain in exchange energy of the triplet configuration $R = 0$, $S = 1$ is overtaken by an increase of kinetic energy and the system makes a transition into a spin singlet lower kinetic energy configuration. Should the dot be asymmetric, the splitting of the two p levels would prevent the formation of the spin triplet configuration.

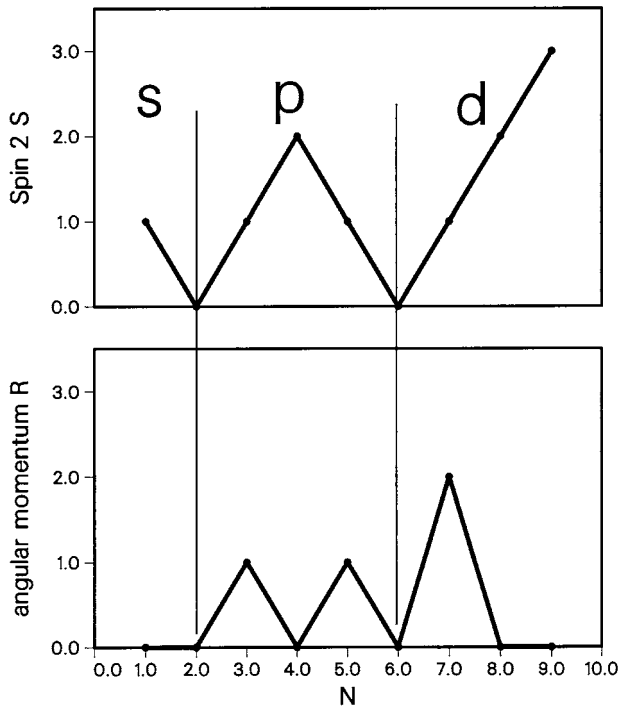

Figure 2. Spin and angular momentum dependence of the ground state of SAD on the number of electrons N.

III. Infra-red spectroscopy

Drexler et al. [7] and Fricke et al. [8] reported FIR absorption measurements of self-assembled dots in a magnetic field. The dots were charged with up to $N = 6$ electrons filling the s and p electronic shells. The infra-red spectroscopy was used to study the electronic excitations of the dots as a function of the number of electrons and the magnetic field.

The excitations of SAD reflect the electronic structure and the number of electrons in the dot. For an

infinite parabolic confinement only the center of mass excitations with frequencies Ω_+ and Ω_- (generalized Kohn's theorem) [1,18] can be measured in FIR. In SAD, a finite number of confined FD levels leads to additional transitions in the IR spectrum related to the magnetic field induced changes in the GS, e.g. spin triplet to spin singlet transition discussed above.

The FIR absorption for N electrons can be conveniently expressed in terms of the FD creation/annihilation operators a and b [17,19]:

$$A(\omega) \propto \sum_f | < f | \sum_{j=1}^{N} (a_j + a_j^\dagger + b_j + b_j^\dagger) i > |^2 \delta(E_f - E_i - \omega), \tag{2}$$

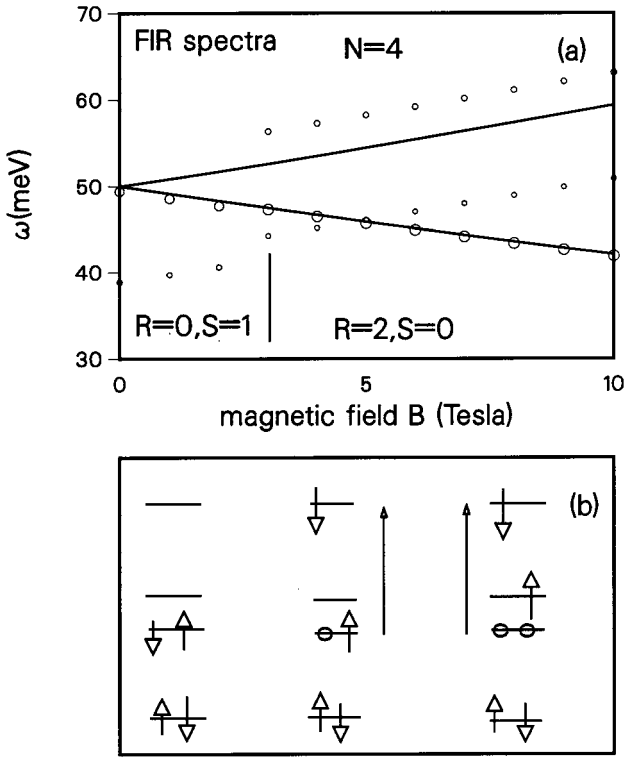

Figure 3. (a) FIR spectra of SAD with N=4 electrons (b) ground state and excited single particle configurations with arrows indicating transitions.

where $|i>$ is the initial (ground) state and the summation is over all bound final states If $f>$. IR radiation connects only the states with the same S_z^{tot} and total angular momenta different by ± 1. We show in Fig. 3a the rmagIletic field evolutions of the IR spectra calculated for the SAD with $N = 4$ electrons. The area of each circle is proportional to the intensity $A(\omega)$. The solid lines show the transition energies $\Omega_\pm$ of the non-interacting system and a vertical line marks the spin transition in the GS. The GS and two excited single particle configurations for $B \geq 2.8T$ are shown in Fig.3b. The two excited configurations responsible for the splitting of the transition for $N = 4, 5$, are coupled through Coulomb interactions. Experiments by Fricke et al. [8] indeed showed the predicted here splitting which illustrates the desired sensitivity of the optical transitions to the number of electrons N.

A. Many excitons in highly excited quantum dots

To understand the operation of a quantum dot based laser one must understand the effect of exciton-exciton interaction on optical properties of highly excited SAD. We shall loosely refer to excitons as interacting electron-hole pairs. Calculations were carried out [13] for SAD with 15 bound states which can be filled with up to 30 electrons and holes [10]. The calculations for up to $N = 6$ electron-hole pairs were carried out exactly and a combination of numerical diagonalization in a partially filled shell and the Hartree-Fock approximation extended calculations up to $N = 20$ excitons. Due to the large confinement, the lowest kinetic energy configurations are an excellent approximation to the ground state in the case of filled shells. When electrons and holes partially fill up a degenerate shell the states and energies are completely determined by their mutual interactions and exact numerical calculations are necessary. However, a simple interpretation of results is possible due to "hidden symmetries" in the problem.

For most quantum dots where electrons and holes are confined in the same physical area, the electron and hole interactions turn out to be symmetrical. For example, in the sample calculated here $v_{ee}/v_{eh} = v_{eh}/v_{hh} =$

1.04. For almost symmetrical interactions, when the Hamiltonian is restricted to a single degenerate shell t, the commutator of the Hamiltonian and the interband polarization operator $P^+ = \sum_i c^+_{i\uparrow} h^+_{i\downarrow}$ can be approximated as $[H_t, P^+] \approx E^t_X P^+$, where $E^t_X = E^e_t + E^h_t - \sum_{j\,k} g_t^{-1} < jjl|V_{eh}|kk >$ is an approximate exciton binding energy. The quantum number $j(-t \leq j \leq t)$ denotes the angular momentum on a given shell. This commutation relation is a manifestation of hidden symmetry [20]. One can construct coherent N exciton states $(P^+)^N|v>$ as eigenstates of P^2. Due to hidden symmetry these states are also eigenstates of the shell Hamiltonian with energies $E(N) = NE^t_X$. The energy of these states is just the sum of energies of noninteracting excitons. These coherent states turn out to be excellent approximations of exact ground states with corresponding overlaps of 100% for shells s and p, and 99.8% and 99.2d and f.

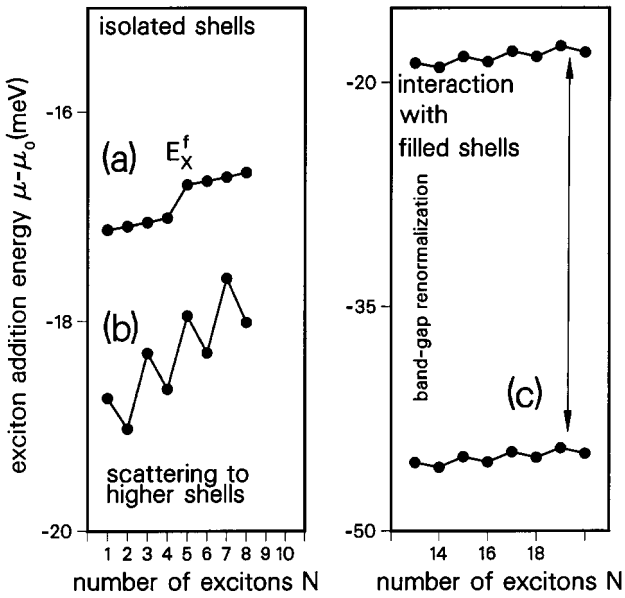

Figure 4. Addition spectrum as a function of the number of excitons (excluding kinetic energy) (a) isolated f-shell (b) f-shell and scattering to g-shell (c) exchange with all filled shells Inset shows the behaviour of the chemical potential, including Coulomb and kinetic energy.

In a QDL one needs to add/subtract an exciton to/from a dot already packed with excitons. In Fig.4a we show the numerically calculated energy to add an exciton to N excitons present in the isolated f shell. The maximum number of excitons in an f shell is $N = 8$. The addition energy is almosta constant, independent of the number of excitons, in agreement with the "hidden symmetry" argument. In Fig. 4b we allow excitons to scatter to higher shells. We see that the addition energy is lowered and that it is split into two lines. The splitting corresponds to the interaction among excitons and is equal to the singlet bi-exciton binding energy in an f shell [13]. Finally, in Fig. 4c we show the same addition energy into the f shell but this time including scattering of excitons in the f shell into empty shells at higher energy and interaction with excitons in filled shells at lower energy. The electrons and holes in filled shells can exchange with those in the f shell. This leads to a sizeable bandgap renormalization. The weak dependence of the chemical potential on the exciton number in a partially filled shell survives. This means that there are steps in the chemical potential of the interacting system corresponding to single-particle shells.

The emission spectrum of exciton droplets corresponds to a spectral function of a "missing" (removed) exciton. This spectral function [13] describes the spectrum of charge excitations of an exciton droplet. The spectral function peaks at the highest energy (chemical potential). Hence the recombination spectrum of highly excited dots, averaged over many different exciton populations with e.g. up to $N = 20$ excitons, will consist of only 4 distinct energies, corresponding to steps in the chemical potential.

An application of the magnetic field destroys the hidden symmetry responsible for this behaviour, as demonstrated by Raymond et al. [10]. The blueshift of the chemical potential was also evident in a SAD red-emitting laser structure studied by Fafard et al. [2]. The interaction of excess electrons with an exciton i.e. the recombination spectrum of modulation doped SADs has been also studied recently [21].

IV. Etched and gated dots in a magnetic field

In gated and etched nanostructures with significant density of surface states, trapped electrons produce long range potential. The effective confining potential is smooth and weak, i.e. of the order of few meV. The effects of electron-electron interactions and magnetic fields are significant [1,22,23]. One can think of electrons as forming quantum Hall droplets, with magnetic field driving the droplets through different filling factors. In the filling factor regime $1 \geq \nu \leq 2$ interesting behavior of the spin polarization is expected [24].

In the filling factor regime $\nu = 1$ the system is expected to form a chiral Fermi liquid. The transitions between different filling factors in this regime involves reconstructions of edges through condensation of edge-magnetorotons [25]. The edge reconstruction is expected to lead to new absorption lines [25]. In the fractional quantum Hall regime the low energy excitations of the droplet are governed by the chiral Luttinger liquid theory [24,26] with non-Fermi liquid behaviour.

A. Magneto-optical measurement of ground state energy

The magnetic field induced transitions of quantum Hall droplets imply changes in the ground state. It turns out that the ground state energy can be measured optically by measuring the mean photon energy $< \omega >$ of the acceptor related recombination line [27]. Experiments in this direction have been reported by Patel et al. [28].

B. Inelastic light scattering by electronic excitations in deep etched quantum dots

Inelastic light scattering measures the excitation spectrum of a QD [29-32] and, in principle, can provide direct evidence of the discrete nature of excitations in zero-dimensional (OD) systems. The electron-electron interactions play a significant role in determining these excitations. For example, in a strong magnetic field the gap in the excitation spectrum of the Hall droplet is determined by electron-electron interactions. The origin of the gap is similar to the origin of the gap in the incompressible Laughlin fluid [22]. Changing the magnetic field leads to a collapse of the gap at special values of the rnagnetic field i.e. to a compressible Hall droplet. One could in principle observe this behaviour as soft modes in Raman spectra [29]. However, the wavelength of the perturbation necessary to excite electrons of the droplet across the gap has to be much smaller then the physical size of the droplet. In typical Raman experiments on 2DEG this wavelength was of the order of few thousand angstroms i.e. much larger than the size of the droplet. Nevertheless, a number of groups [30,31] have undertaken inelastic light scattering of quantum dots. In the absence of a magnetic field, Strentz et al. [30] measured the resonant electronic Raman spectrum from shallow etched QD's with sizes down to 400nm. Lockwood et al. [31] measured the resonant electronic Raman spectrum of deep etched modulation-doped QD's with sizes down to lOOnm and in a magnetic field. Both groups attributed observed structures in the Raman spectra to the OD density of states. These observations were possible due to patterning, and hence surface roughness, of the samples.

The samples studied by Lockwood et al. [31] were GaAs/GaAlAs quantum dots prepared in the form of disks of radius R. Disks with radii in the range $50nm < R < 100nm$ were etched from a modulation doped multi-quantum well structure [32] with carrier density $n_s = 8.5 \cdot 10^{11}\mathrm{cm}^{-2}$. The near-resonant electronic Raman spectra (in a backscattering geometry) were measured in magnetic fields up to 12 T at 2K.

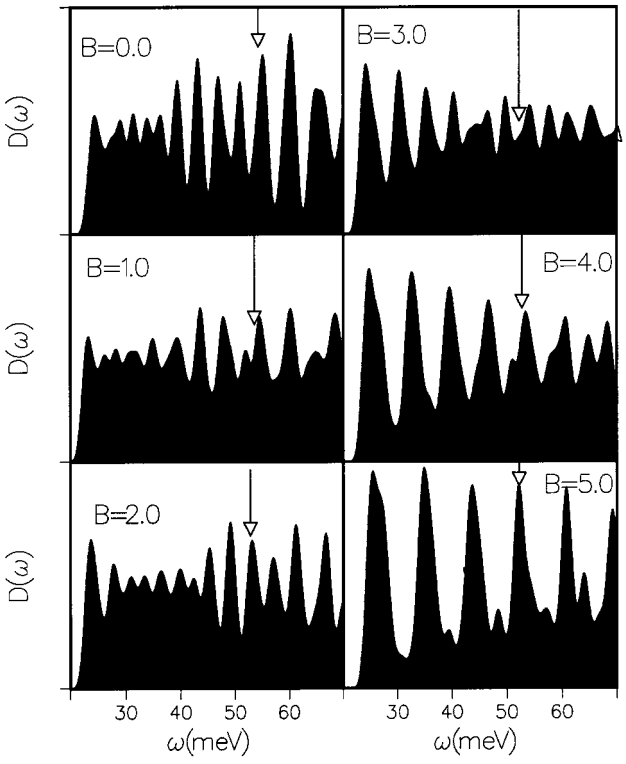

Figure 5. Calculated density of states of a dot with carrier density $n_s = 8.0 \cdot 10^{11}\mathrm{cm}^{-2}$ (N=124) and radius $r = 70$nm for different values of the magnetic field.

To calculate the wavefunctions, energies and single particle excitation(SPE) spectra we approximate the quantum dots as disks of radius R and thickness t, confined by infinite potential barriers. The positive charges of ionized donors are modeled as a disk with uniform density, separated by a distance d from the plane of the

dot. For such a high density multiple- quantum well system, we assumed that electrons trapped in surface states represent a very small fraction of the free electrons.

In the Hartree approximation, the many electron Hamiltonian for free electrons is replaced by a Hamiltonian of a single particle moving in confining potential and a self- consistent Hartree potential determined by the electronic and the positive charge density through electron-electron and electron-positive charge Coulomb interactions. The electron density is given in terms of occupied eigenstates Ψ_ν^m of the Hartree Hamiltonian, where m determines angular momentum and ν labels states with this angular momentum. In numerical solution of the Hartree equations the following parameters were used: $R = 70nm$, $N_e = 124$, $d = 30nm$, $t = 8nm$. These parameters correspond to a disk with diameter of 140nm and density $n_S \approx 8 \cdot 10^{11}$ cm^{-2}. In calculating Coulomb interactions we have also assumed a uniform dielectric constant of GaAs and neglected the effects due to image charges associated with the semiconductor-vaccum interface. The calculated Hartree density of states(DOS) for different values of the magnetic field is shown in Fig.5. The Hartree energy spectrum is discrete and hence the OD density of states (DOS) consists of a series of peaks. For $B = 0$ there is a typical single particle energy spacing $\delta E \approx 0.1 - -0.5meV$ within each peak and an overall arrangement of peaks in the DOS reminiscent of the shell structure of atoms, with a typical energy spacing of $\approx 5meV$. When compared with the DOS of noninteracting electrons we find that the modulation is enhanced by electron-electron interactions. This is due to the spatial separation of the positive background from the disk. Since electrons repel each other very effectively, the electron charge density is depressed inside the disk and enhanced at the edges of the disk. The Hartree potential is therefore repulsive in the center of the dot, a situation very similar to Hartree potentials in modulation doped quantum wells. The shell structure is enhanced by the degeneracy of states with the same absolute value of angular momentum m. This degeneracy is removed by magnetic field, leading to a splitting of energy levels. For small values of the magnetic field a rapid rearrangment and crossing of levels takes place. For higher magnetic fields, $B > 4T$, Landau bands begin to form.

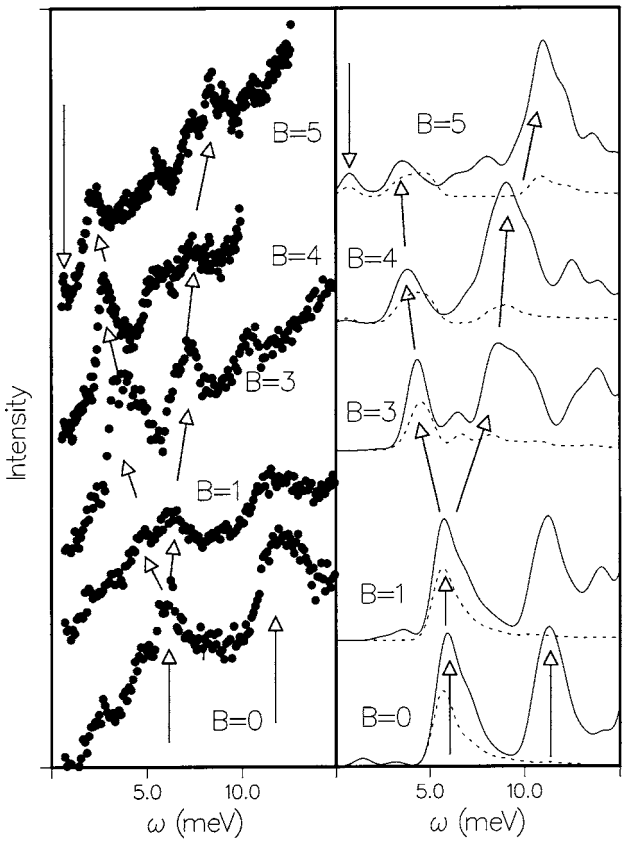

Figure 6. (a) measured Raman spectra of quantum dots with nominal carrier density $n_s = 8.5 \cdot 10^{11}$cm^{-2} and radius $r = 75$nm for magnetic fields B = 0 - 5T. (b) calculated SPE spectra $I(q, \omega)$ of a dot with carrier density $n_s = 8.0 \cdot 10^{11}$cm^{-2} (N=124) and radius $r = 70$nm and $q = 1 \cdot 10^5$cm^{-1} (dashed line) and $q = 5 \cdot 10^5$cm^{-1} (solid line). The arrows point out related peaks in experiment and theory for each magnetic field.

Experimental Raman spectra for a dot with a nominal radius $R = 75nm$ and nominal density $n_s = 8.5 \cdot 10^{11}$cm^{-2} in magnetic fields $B = 0 - 5T$ are shown in Fig.6a. The $B = 0$ spectra show clearly broad peaks separated by approximately $\omega_0 = 6meV$ as indicated by arrows. Up to three peaks were observed. On top of the broad structure a number of sharper peaks, especially at low energies, is also visible. As the magnetic field increases, the spectrum evolves in a complicated way. For example, the lowest peak appears to split and evolve into two peaks $\Omega_{+/-}$ as indicated by arrows. However, the Ω_+ peak at $B = 5$ T is split into a number of peaks, and an additional low energy peak appears. This complicated behavior can only be understood by a comparison of experiment with realistic calculations of Raman spectra. The Raman spectra can be divided into three

classes: charge density excitations(CDE), spin density excitations(SDE), and single particle excitations(SPE). Both CDE and SPE are simple a linear combination of excited states, and follow the SPE. The CDE and SPE can be distinguished by the polarization dependence of the scattered light. However, since the exciting light is scattered by a 2D array of pillars, the spectra do not show the wavevector conservation and clear polarization dependence found in quantum well experiments [33]. In the interpretation of the experimental spectra, we restricted ourselves to the analysis of the dominant SPE based on Hartree calculations. In the absence of the wavevector conservation the cross section $I(\omega)$ is averaged over all possible wavevector transfers $q = k_f - k_i$ of the incident (k_f) and scattered(k_f) light: $I(\omega) \approx \sum_q W(q) I(q,\omega)$. The function $W(q)$ depends on the structure of individual dots and the structure of an array of pillars on the sample surface. The Raman cross section $I(q,\omega)$ for a given wavevector transfer q and frequency ω is proportional to the imaginary part of the polarizability $\Pi(q,\omega)$ of the system [34]:

$$I(q,\omega) \approx \sum_{m,m',\nu,\nu'} |< m',\nu'|\rho_q|m,\nu >|^2 (1 - f(m',\nu')) f(m,\nu) \delta(E^{\nu'}_{m'} - E^{\nu}_{m} - \omega), \quad (3)$$

where the density operator $\rho_q = e^{i\vec{q}\vec{r}}$, and $f(m,\nu)$ is the Fermi occupation function for a state ν with angular momentum m and energy E^{ν}_{m}. The coupling through the density fluctuation operator $e^{i\vec{q}\vec{r}} = \sum_m i^m e^{im\theta} J_m(qr)$ induces transitions between different angular momenta m and different single particle states ν.

We summarize in Fig.6b the evolution with magnetic field of calculated SPE Raman spectra. In the right panel of Fig.3 we show representative calculated SPE spectra for small ($qR = 0.7$; $q = 1 \cdot 10^5 \mathrm{cm}^{-1}$) and large ($qR = 3.5$; $q = 5 \cdot 10^5 \mathrm{cm}^{-1}$) wave-vectors involved in the scattering process. For comparison with experiment the calculated energies have been multiplied by a factor of 1.3 to account for a decrease in the effective dielectric constant due to the vacuum. The calculated spectra for $q = 1 \cdot 10^5 \mathrm{cm}^{-1}$ and $B = 0$ show only one peak while spectra for $q = 5 \cdot 10^5 \mathrm{cm}^{-1}$ consist of three main transitions with a spacing of the order of 6meV in good agreement with experiment. If we follow the evolution of the calculated SPE spectrum as a function of the magnetic field we see that the $q = 5 \cdot 10^5 \mathrm{cm}^{-1}$ spectra are in agreement with the measured spectra. For example, at B=1T we see two peaks, while at B=3T we see three peaks. At B=5T the agreement is also encouraging, especially with respect to the emergence of a very low energy excitation associated with the Fermi level crossing a quasi-Landau level band. The measured spectra are, of course, an average over many such calculated spectra.

In summary, the experimental spectra show a magnetic field behavior consistent with that calculated for single particle excitations within the Hartree approximation. The excitation spectrum reflects the formation of electronic shells within quantum dots and exhibits a complex evolution with magnetic field. This now opens up the possibility to study collective excitations from a range of strongly correlated ground states in QD's in a strong magnetic field [24,29].

V. Conclusions

The ground state properties and charge and spin excitations in self-assembled and deep etched dots were obtained through exact diagonalization techniques, Hartree-Fock, and Hartree calculations. The calculations of far infrared, interband, and inelastic light scattering spectroscopies were compared with experiments.

Acknowledgments

Collaboration with A. Wojs, J. A. Brum, D. J. Lockwood, S. Fafard, S. Raymond, A. Pinczuk, and M.

Potemski on various aspects of this work is acknowleadged.

References

1. For recent reviews and references see M. Kastner, Physics Today, **24**, January 1993; T. Chakraborty, Comments in Cond. Matter Physics **16**, 35 (1992); R. C. Ashoori, Nature **379**, 413 (1996).
2. S. Fafard et al. Science **274**, 1350 (1996).
3. P. M. Petroff and S. P. Denbaars, *Superlattices and Microstructures* **15**, 15 (1994); for a recent review see Proceedings of International Conference on Modulated Semiconductor Structures, Madrid, 1995.
4. M. Grundmann, et. al, Phys. Stat. Sol. **188**, 249 (1995).
5. J. Y. Marzin, G. Bastard, Solid State Comm. **92**, 437 (1994).
6. R. Notzel,et. al, Appl.Phys.Lett. **66**, 2525 (1995).
7. H. Drexel, et. al, Phys. Rev. Lett. **73**, 2252 (1994).
8. M. Fricke, A. Lorke, J. P. Kotthaus, G. Medeiros-Ribeiro, and P. M. Petroff, Europhys. Lett. **36**, 197 (1996).
9. S. Fafard, et. al, Appl. Phys. Lett. **65**, 1388 (1994); R. Leon, et. al, Appl. Phys. Lett. **67**, 521 (1995); S. Fafard, et. al, Phys. Rev. B **52**, 5752 (1995).
10. S. Raymond, S. Fafard, P. J. Poole, A. Wojs, P. Hawrylak, S. Charbonneau, D. Leonard, R. Leon, P. M. Petroff, and J. L. Merz, Phys. Rev. B, **54**, 11 548 (1996). S. Raymond et al, Solid State Commun. (in press)
11. A. Wojs, P. Hawrylak, S. Fafard, L. Jacak; Phys. Rev. B, **54**, 5604 (1996).
12. A. Wojs and P. Hawrylak, Phys. Rev. B, **53**, 10 841 (1996)
13. A. Wojs and P. Hawrylak, Solid State Comm. **100**, 487 (1996). P. Hawrylak and A. Wojs, Proceedings of International Winter School in Solid State Physics, Mauterndorf, 1996.
14. U. Bockelmann, et al. Phys. Rev. Lett. **76**, 3622 (1996).
15. M. Bayer, et. al, Phys. Rev. Lett. **74**, 3439 (1995).
16. A. Wojs and P. Hawrylak, Phys. Rev. B **51**, 10 880 (1995).
17. P. Hawrylak, Solid State Comm. **88**, 475 (1993).
18. W. Kohn, Phys. Rev. **123**, 1242 (1961); L. Brey, N. Johnson, B. Halperin, Phys. Rev. B **40**, 10 647 (1989); P. Maksym, T. Chakraborty, Phys. Rev. Lett. **65**, 108 (1990).
19. D. Pfannkuche, V. Gudmundsson, P. Hawrylak, R. R. Gerhards, Solid State Electronics **37**, 1221 (1994).
20. I. V. Lerner, Yu. E. Lozovik, Zh. Eksp. Teor. Fiz.**80**, 1488 (1981) [Sov. Phys. JETP **53**, 763 (1981).]; D. Paquet, T. M. Rice, K. Ueda, Phys. Rev. B, **32**, 5208 (1985); A. H. MacDonald, E. H. Rezayi, Phys. Rev. B **42**, 3224 (1990); Yu. A. Bychkov and E. I. Rashba, Phys. Rev. B, **44**, 6212 (1991).
21. A. Wojs and P. Hawrylak, submitted to Phys. Rev. B.
22. P. Hawrylak, Phys. Rev. Lett. **71**, 3347 (1993).
23. R. C. Ashoori, et. al, Phys. Rev. Lett. **71,** 613 (1993).
24. A. Wojs and P. Hawrylak, submitted to Phys. Rev. B
25. P. Hawrylak, A. Wojs, and J. A. Brum, Solid State Commun. **98**, 847 (1996); Phys. Rev. B, **54**, 11 397 (1996).
26. X. G. Wen, Phys. Rev. B **41**, 12 838 (1990); C. de Chamon and X.-G. Wen, Phys.Rev. B**49**, 8227 (1994).
27. P. Hawrylak and D. Pfannkuche, Phys. Rev. Lett. **70**, 485 (1993).
28. S. Patel, A. S. Plaut, P. Hawrylak, H. Lage, P. Grambow, D. Heitmann, K. von Klitzing, J. P. Harbison and L. T. Florez Solid State Comm. (in press).
29. P. Hawrylak, Solid State Commun. **93**, 915 (1995).
30. R.Strentz et al., Phys. Rev. Lett. **73**, 3022 (1994).
31. D. J. Lockwood, P. Hawrylak, P. D. Wang, C. M. Sotomayor-Torres, A. Pinczuk, and B. S. Dennis, Phys. Rev. Lett. **77**, 354 (1996).
32. P. D. Wang et al., Superl. and Microstr. **15**, 23 (1994).
33. C. Dahl et al., Phys. Rev. B**51**, 17211 (1995).
34. A. Pinczuk and G. Abstreiter in *Light Scattering in Solids*, edited by M. Cardona and G. Guntherodt (Springer,Berlin 1989)p.153; P. Hawrylak et al., Phys. Rev. B**32**, 5169 (1985).